Design and analysis of a multi-cell subscale tank for liquid hydrogen storage

Tapeinos, I; Koussios, S; Groves, RM

DOI
10.1016/j.ijhydene.2015.10.104

Publication date
2016

Document Version
Accepted author manuscript

Published in
International Journal of Hydrogen Energy

DESIGN AND ANALYSIS OF A MULTI-CELL SUBSCALE TANK FOR LIQUID HYDROGEN STORAGE

Ilias G. Tapeinos[1], Sotiris Koussios[1] and Roger M. Groves[2]

[1]Structural Integrity & Composites Group, Faculty of Aerospace Engineering,
Delft University of Technology, Kluyverweg 1, 2629HS Delft, Netherlands
[2]Aerospace Non-Destructive Testing Laboratory, Faculty of Aerospace Engineering,
Delft University of Technology, Kluyverweg 1, 2629HS Delft, Netherlands

Email: I.Tapeinos@tudelft.nl, web page: http://www.tudelft.nl/

ABSTRACT

This paper outlines the structural performance of a conformable pressurizable tank consisting of intersecting spherical shells (multi-cell tank). Multi-cell tanks outrival conventional multiple cylindrical tanks in volumetric efficiency when required to fit in a rectangular envelope in the automotive industry. When pressurized, the multi-cell (or multi-bubble) tank experiences high stress concentrations at the vicinity of the junctions, and thus the concept of effectively reinforcing those regions without adding significant excess weight becomes crucial. Furthermore, when applied for cryogenic medium storage, the heat transfer between different bodies and the generation of respective thermal stresses in such vessels makes the solution more complicated. In this paper the effect of the i) fiber-reinforced materials at the membrane and ii) unidimensional carbon tows at the intersections on the structural integrity of the tank is analysed for different loading scenarios. An operating window for the proposed tank configuration under the given loading scenario is established indicating the safe zone where the tank can operate.

Keywords: Conformable tanks; Thermal stresses; Finite element method

1 INTRODUCTION

In the aerospace hydrogen containment field, tanks are required to have a high internal volume- in a pre-defined allowable space. The EU CHATT (Cryogenic Hypersonic Advanced Tank Technologies) project deals with investigating the use of carbon-fibre reinforced plastics (CFRP) for type IV liquid hydrogen (LH_2) tanks in the two-stage hypersonic reusable launch system (RLV) Space-Liner [1]. Throughout operation the tank is subjected to various combined loading cases that involve inner pressure and temperature changes as well as gravitational accelerations induced by the RLV.

Multi-cell pressure vessels have shown the potential of higher volumetric efficiency -within a rectangular envelope- compared to conventional cylindrical tanks [2]-[3]. They consist of rows of spherical cells joined together at appropriate intersections. Spherical membrane cells enable the structure to be loaded in uniform equal biaxial tension, which enables structural efficiency maximization [4]. Additionally spheres are the most favorable shapes for pressure vessels stress-wise, as well as having the maximum volume and minimum surface area, thus lowest material requirement. The use of intersecting pressure tanks has been reported in several published works, ranging from automotive fuel tanks [3] to deep-submerged pressure hulls [5]-[6]. The only reported application multi-cell vessels with fiber-reinforced materials for cryogenic fuel storage was the X–33 LH_2 tank, consisting of a multi-lobed and linerless configuration with integrally bonded, woven composite joints [7].

For the case of cryogenic tanks, thermal insulation systems are employed- in order to minimize the liquid fuel boil-off rate [8]-[9]. T.C. Nast et. al. studied the sensitivity of boil-off to multi-layer insulation (MLI) thermal conductivity [10]. However, the main focus of most published works has been to estimate the temperature gradient through-the-thickness of the shell and determine respective

fuel loss, rather than isolating the effect of different insulation configurations on thermal stresses and thus tank performance [11].

Additionally, a plastic liner is generally employed in a composite overwrapped vessel (a Type IV vessel), in order to prevent boiled-off gas leaking through the wall, and to reduce weight compared to Type III vessels that utilize a metal liner. However, differences in the values of the coefficient of thermal expansion (CTE)- between the liner and the tank wall can lead to thermal stresses and even separation under a particular temperature gradient. Therefore, besides permeability resistance, the two driving properties for liner material selection are i) the CTE compatibility with the composite tank wall and ii) the modulus of elasticity, since the liner must be flexible enough to be pressed against the tank wall surface in order to transfer the pressure load. However, a safe operating window for plastic-lined tanks of such geometry has not yet been established and is hereby present in the current work.

In the present work, a trade-off design study of plastic-lined multi-cell tank concepts has been performed in terms of evaluating their structural performance- under a given loading scenario, both analytically and with the use of Finite Element Analysis (FEA). The effect of the reinforcement of the intersections on the tank behavior was evaluated. Furthermore, a coupled temperature-displacement FE analysis was employed to investigate heat transfer phenomena between the liner, the tank wall and the surrounding environment, as well as to evaluate respective thermal stresses. Different insulation systems were analysed based on their effect on the arising shell stresses and strains. Finally, an operating window for the case of thermo-mechanical loading was established for the proposed tank design indicating the safe zone where the tank can operate.

2 TANK OPERATION REQUIREMENTS

To ensure safety and acceptance, pressurized fuel tanks are always subject to strict design and verification requirements. Throughout operation in the Space-Liner, the LH_2 tank will be subjected to various combined loading cases such as inner pressure and temperature change -due to the stored medium being at cryogenic temperatures- as well as gravitational accelerations induced by the RLV [12].

Figure 1 depicts the different LH_2 tank loading scenarios induced at the tank throughout the RLV flight, which were considered as load reference scenario in this study. These load cases are associated with i) nominal cryogenic operation at maximum expected temperature or ii) nominal empty operation after main-engine-cut-off (MECO) and iii) off-nominal operation after early MECO with remaining LH_2 inside. The service pressure of 0.38 [MPa] (in the first case) which together with a safety factor of 1.5 and internal temperature of -253[^{o}C] are the most significant tank design constraints. An integral part of the design is to reinforce the LH_2 tank, in order to be able to withstand service loads. The application of CFRP at the tank wall will provide support to the structure, due to its high specific strength and stiffness. Symbols P_{ull} and P_{bottom} refer to the pressures of the unfilled (ullage) and filled -with liquid- tank areas respectively, while T_{in} and T_{ext} represent the tank internal and external temperatures. Finally n_x and n_z are the axial and radial gravitational accelerations induced at the LH_2 tank by the RLV.

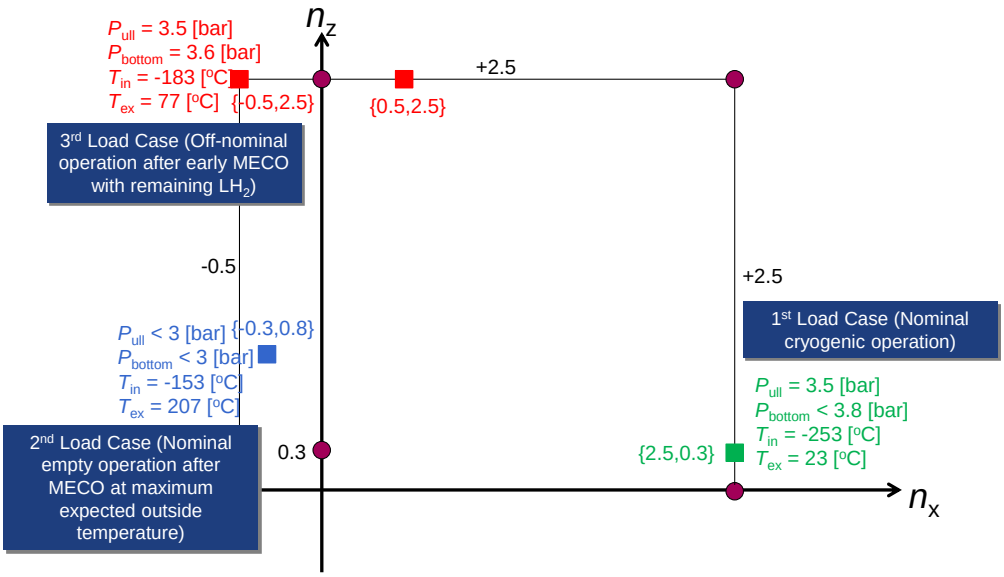

Figure 1: Simplified flight load cases of the Space Liner LH_2 tank.

Figure 2 shows the expected benefits in terms of volumetric efficiency of the conformable tank concept as compared to multiple cylinders in a rectangular envelope in the automotive industry [3]. The cross sections of the tanks are depicted, and for various aspect ratios (envelope length/width) the conformal vessel concept surpasses the respective cylindrical one in terms of volumetric efficiency. Throughout this study a sub-scale of the actual tank (under consideration) was designed and analysed.

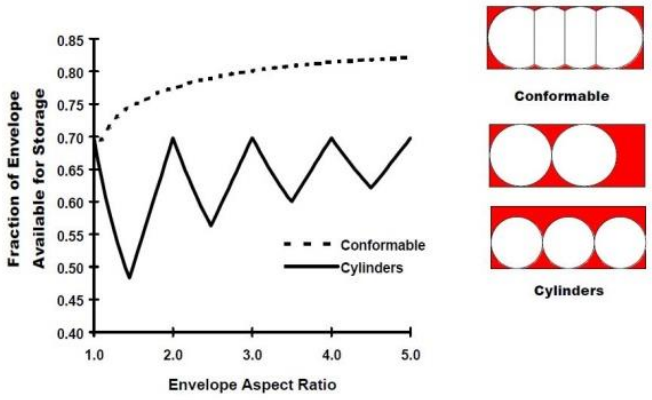

Figure 2: Comparison of the volumetric efficiency between i) cylindrical and ii) conformable tanks in a rectangular envelope [3].

Furthermore, the sub-scale design must be consistent with the manufacturing processes of the liner and tank wall. More specifically, the external contour of the designed subscale conformal tank must be feasible to manufacture with a moulding process (e.g. roto-moulding), without inducing any imperfections at narrow sections, such as membrane junctions. Additionally, an effective manufacturing process should be employed for the application of the composite plies on top of the liner.

3 SUB-SCALE TANK STRUCTURAL CONFIGURATIONS

This section deals with isolating the different loading scenarios of interest and analyzing their effect on various tank aspects of the proposed design.

3.1. Spherical Membranes

3.1.1 Inner Pressure

Figure 3a depicts a conceptual design of the structure of interest, which is a quadri-spherical tank, with all centroids in the same plane. As can be seen in Figure 1, the inner normal pressure -induced by the stored liquid medium on the tank wall- can be considered as uniform. Symbol F_a is the resultant applied axial force on the polar opening, r is the shell radius, z is the shell's height coordinate and β is the inclination angle of the meridional profile at a particular point. It is expected that the pressure load induced at the vicinity of any intersection is partially carried by the membrane and partially by the reinforcement placed at the intersection, where the stress concentrations obtain their highest values.

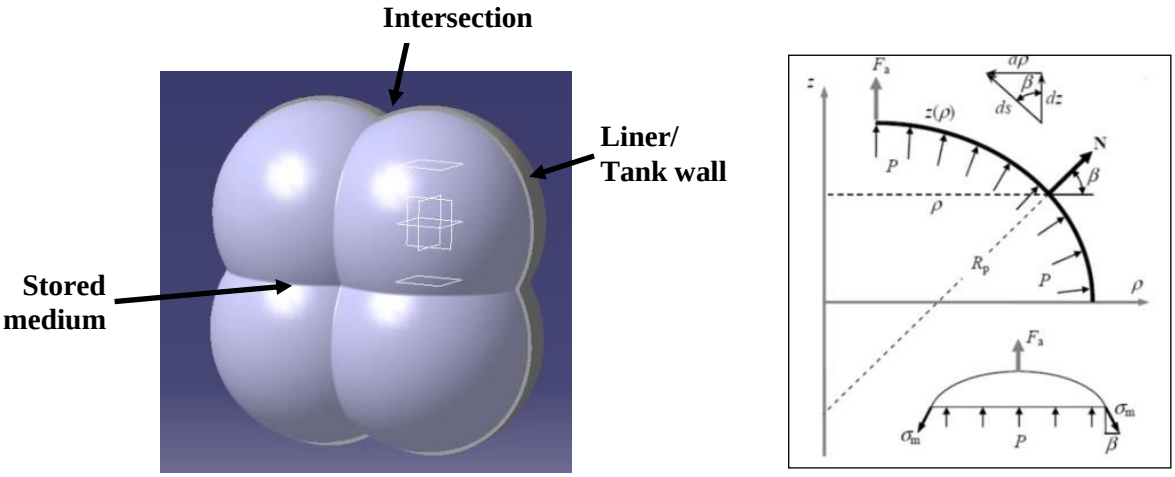

Figure 3: a) Quadri-spherical tank with equal shell radius for all cells and b) stresses equilibrium on a shell of revolution.

In order to derive the stress environment of the multi-bubble configuration, the membrane theory for pressure vessels is utilized for the spherical membranes. It relies on the equilibrium of in-plane stresses on a membrane element by neglecting any bending moments. The average membrane stress values can be derived by dividing the membrane force with the respective shell thickness. Figure 3b depicts a shell of revolution, which is obtained by rotating a curve (meridian) about an axis of revolution. Therefore an element of the reference surface of the shell is formed by two adjacent meridians and two parallel circles. More specifically, the in-plane equilibrium condition is provided below [13]:

$$\frac{P}{t} = \frac{\sigma_m}{R_m} + \frac{\sigma_p}{R_p} \tag{1}$$

where P is the internal pressure, R_m is the radius of curvature of the meridian, R_p is the radius of curvature in the parallel direction, t is the shell thickness and σ_m, σ_p are the in-plane shell stresses in the meridian and parallel directions respectively while v_{xy} is the ply Poisson's ratio. The in-plane shear stress is equal to zero due to the uniform strain condition. Since composite plies are employed at the membrane, the stiffness matrix of a layer at the tank wall ($\mathbf{C}_o$) can be derived from:

$$\mathbf{C}_o = \begin{pmatrix} \dfrac{E_x}{1-\nu_{xy}\nu_{yx}} & \dfrac{\nu_{xy}E_y}{1-\nu_{xy}\nu_{yx}} & 0 \\ \dfrac{\nu_{xy}E_y}{1-\nu_{xy}\nu_{yx}} & \dfrac{E_y}{1-\nu_{xy}\nu_{yx}} & 0 \\ 0 & 0 & G_{xy} \end{pmatrix} \tag{2}$$

where $\nu_{yx} = \dfrac{\nu_{xy}E_y}{E_x}$ and E_x, E_y and G_{xy} are the ply tensile moduli parallel and transverse to the fibers, and the shear modulus respectively. A quasi-isotropic stacking sequence was chosen ($[0,45,-45,90]_s$), thus obtaining equal stiffness at all in-plane directions. Therefore the resulting stiffness of the laminate will be derived from [14]:

$$\mathbf{C}_{\text{lam}} = \frac{1}{\sum_{k=1}^{n} t_{\text{ply}}} \cdot \sum_{k=1}^{n} \mathbf{C}(\theta) \cdot t_{\text{ply}} \tag{3}$$

where:

$$\mathbf{C}(\theta) = \mathbf{M}(\theta) \cdot \mathbf{C}_o \cdot \mathbf{M}^{\mathrm{T}}(\theta) \text{ and } \mathbf{M}(\theta) = \begin{pmatrix} \cos^2\theta & \sin^2\theta & \sin(2\theta) \\ \sin^2\theta & \cos^2\theta & -\sin(2\theta) \\ -\cos(\theta)\sin(\theta) & \cos(\theta)\sin(\theta) & \cos(2\theta) \end{pmatrix} \tag{4}$$

where θ represents the different lamina angles, t_{ply} is the ply thickness, n the number of angles, $\mathbf{M}(\theta)$ is the stress transformation matrix and $\mathbf{C}(\theta)$ is the transformed (reduced) ply stiffness matrix. As a result, the shell stresses vector is given by multiplying the laminate stiffness matrix by the shell strains vector:

$$\begin{Bmatrix} \sigma_m \\ \sigma_p \\ 0 \end{Bmatrix} = \mathbf{C}_{lam} \cdot \begin{Bmatrix} \varepsilon_m \\ \varepsilon_p \\ 0 \end{Bmatrix} \tag{5}$$

where ε_m and ε_p are shell strains at meridional and transverse directions. Finally the layer stresses at the material coordinate system are given by:

$$\begin{Bmatrix} \sigma_1 \\ \sigma_2 \\ 0 \end{Bmatrix} = \mathbf{C}_o \cdot (\mathbf{M}^T(\theta))^{-1} \cdot \mathbf{S}_{\text{lam}} \cdot \begin{Bmatrix} \sigma_m \\ \sigma_p \\ 0 \end{Bmatrix} \tag{6}$$

where $\mathbf{S}_{\text{lam}} = (\mathbf{C}_{\text{lam}})^{-1}$ is the laminate compliance matrix. Due to axial and shell force equilibrium:

$$\sigma_m = \frac{PR_p}{2t}(F_a + 1) \ , \ \sigma_p = \sigma_m \left(\frac{2}{F_a + 1} - \frac{R_p}{R_m} \right) \tag{7}$$

where F_a is derived from:

$$F_a = \sigma_m (2\pi\rho t)\cos\beta - P\pi\rho^2 \tag{8}$$

where ρ is the radius at any given parallel of the shell. For spherical elements and away from the polar opening, the following conditions are applied: i) $R_p = R_m$ and ii) $\sigma_m = \sigma_p$.

By utilizing the Tsai-Wu failure criterion (Eq.9) the strength values of the spherical elements can be calculated for the tank wall material and the lay-up under consideration:

$$f_1\sigma_1 + f_2\sigma_2 + f_{11}\sigma_1^2 + f_{22}\sigma_2^2 + f_{66}\tau_6^2 + 2f_{12}\sigma_1\sigma_2 = 1 \tag{9}$$

where $f_1 = \frac{1}{X_t} - \frac{1}{X_c}$, $f_{11} = \frac{1}{X_t X_c}$, $f_2 = \frac{1}{Y_t} - \frac{1}{Y_c}$, $f_{22} = \frac{1}{Y_t Y_c}$, $f_{66} = \frac{1}{S^2}$, $f_{12} = -\frac{1}{2}\sqrt{f_{11} f_{22}}$ while the respective X_t, X_c, Y_t, Y_c and S ply strength values of HexPly AS4/8552 can be found in Table1. This failure criterion will enable establishing an operating window of the proposed tank design, based on first-ply-failure (FPF).

Table 1: Tank wall material properties (AS4/8552).

ELASTIC PROPERTIES					STRENGTH				
E_x (GPa)	E_y (GPa)	G_{xy} (GPa)	ν_{xy}	t_{ply} (mm)	X^t (MPa)	X^c (MPa)	Y^t (MPa)	Y^c (MPa)	S (MPa)
133	9.13	5.21	0.3	0.19	2178.2	1783.5	91.7	340.9	129.1

3.1.2 Thermal Loading

I. Temperature Distribution

It is of significant importance to calculate the arising temperatures at the spherical cells (liner & tank wall) due to fact that the shell structure under study is meant for cryogenic medium storage. More specifically, since fibre-reinforced composite plies are draped on the liner top surface while the tank is subjected to different internal and external temperatures (Figure 1), evaluating the heat transfer from one body to another will enable the estimation of temperature gradients through-the-thickness and thus allow the calculation of the involved thermal strains and stresses. When the liner is in contact with the tank wall, the tangential behavior at the interface is governed by normal forces and the analysis consists of heat conduction between those two bodies and convection with air at the external surface of the tank configuration.

The thermal conductivity values of the tank wall and the liner materials are required for the calculations. While the liner material is considered as isotropic, fiber-reinforced materials exhibit anisotropy, with the principal directions of the thermal conductivity being parallel and perpendicular to the fibre orientations. Table 2 shows the thermal conductivity values of the liner and tank wall materials.

Table 2: Thermal Conductivity of liner and tank wall materials.

Property		PA	AS4/8552 (Axial)	AS4/8552 (Transverse)
k	[W K^{-1} m^{-1}]	0.22	3.972	0.3363

A temperature gradient only through-the thickness (one-dimensional heat transfer) of the spherical cell is considered. For the differential control volume of a spherical shell it is required that $q_r = q_{r+dr}$ for steady-state under one-dimensional conditions with no heat generation, where q_r and q_{r+dr} are the heat rates at different points through-the-thickness. The appropriate form of Fourier's law is:

$$q_r = -kA\frac{dT}{dr} = -k(4\pi r^2)\frac{dT}{dr} \tag{10}$$

where $A = 2\pi r$ is the area normal to heat transfer direction and r and T are the radius and temperature at any given point through-the-thickness of the sphere. Since for steady-state conditions q_r is constant

and independent of r the equation above can be expressed in its integral form, assuming that k is constant:

$$q_r = \frac{4\pi k(T_{in} - T_{out})}{\left(1/r_{in}\right) - \left(1/r_{out}\right)} \tag{11}$$

where T_{in} and T_{out} are the internal and external shell temperatures and r_{in} and r_{out} are the inner and outer radiuses of interest respectively.

For the case of natural convection at the external surface the following heat rate is defined by:

$$q_{conv} = hA(T_s - T_\infty) \tag{12}$$

where T_s and T_∞ is the surface and air temperatures respectively, while h is the heat transfer coefficient that can be derived from $h = Nuk_{air} / r_{out}$, with Nu, k_{air} and r_{out} being the dimensionless Nusselt number, air conductivity and shell external radius respectively. However, the following expression must be employed, in order to derive the Nusselt number for a sphere [15]:

$$Nu = \left(2 + \left(0.56\left(\frac{\Pr}{0.846 + \Pr}\right)Ra\right)^{1/4}\right) \tag{13}$$

where Pr is the dimensionless Prandtl number (in the case of air it is considered as 0.7) and Ra is the dimensionless Rayleigh number (for the case of cooling) given by the expression below:

$$Ra = \frac{g(2r_{out})^3 \beta(T_\infty - T_s)}{va} \tag{14}$$

where g is the gravitational acceleration, β is derived from $1/T_\infty$ and v and a are the air kinematic viscosity and thermal diffusivity respectively. The values of entities k_{air}, v and a were considered as functions of temperature in this study. The inner surface of the tank is assumed to obtain a uniform temperature value, equal to the inner temperature values given in Figure 1.

Finally the temperature distribution can be given by solving equations 11 and 12 for heat rate equilibrium through-the thickness of the spherical cell. The following equation is used for a spherical cell through-thickness once the temperature at the body boundaries is known:

$$\bar{T} = T_{in} - \Delta T \frac{(1 - r_{in}/r)}{(1 - r_{in}/r_{out})} \tag{15}$$

II. Thermal Stresses & Strains

As mentioned above, the liner/tank wall contact depends on the rate of expansion and contraction of each body which is dominated by the inner pressure, as well as tank inner and outer temperature. It is necessary for the liner to be pressed against the tank wall surface, in order to transfer the pressure load to the tank wall. However, in the given load regime, the tendency is for the liner and tank wall to form a gap due to different coefficients of thermal expansion and because of the temperature difference on the inside and outside of the tank. Therefore materials that limit this behaviour should be employed for the liner or an effective insulation layer must be added, in order to alternate to the temperature and thus strain distribution at both bodies.

As a result, the behaviour of the liner and tank wall is analysed by estimating their hoop strain values when subjected to both thermal and mechanical loading. There are two distinct cases: the first case is for the two bodies to behave independently and therefore the interfacial contact is not forced and the second case is to assume that the liner is tied to the tank wall, thus making sure that they the two bodies are in contact, no matter what level of thermal loading is present.

For the first multi-layered case the equal axial and transverse stresses and strains at the liner can be calculated by Equations 16 and 17 respectively [16]:

$$\sigma_{\theta\theta,\varphi\varphi} = \frac{Pr}{2t} + \left[\frac{aE_{\text{liner}}}{(1-\nu_{\text{liner}})r^2}\right]\cdot\left[\left(\frac{r^2+r_{\text{in}}^2}{r_{\text{out}}^2-r_{\text{in}}^2}\right)\cdot\int_{r_{\text{in}}}^{r_{\text{out}}}\bar{T}\,r\mathrm{d}r + \int_{r_{\text{in}}}^{r}\bar{T}\,r\mathrm{d}r - \bar{T}\,r^2\right] \tag{16}$$

$$\varepsilon_{\text{liner}} = \left(\frac{1}{E_{\text{liner}}}\right)\cdot(\sigma_{\theta\theta}-\nu_{\text{liner}}\sigma_{\theta\theta}) + a\cdot(\bar{T}-T_{\text{initial}}) \tag{17}$$

Under the case of tied liner and tank wall, there should a strain compatibility, according to which the hoop strains of the both layers (tank wall, liner) should be the same. The equation below is used to calculate the hoop strain for the case of tied liner and tank wall and shows the effect of the material properties and temperature differences [17]:

$$\varepsilon_{\text{hoop}} = \frac{A_{\text{liner}}E_{\text{liner}}a_{\text{liner}}\Delta\text{T}_{\text{inner}}(\nu_{\text{comp}}-1) + A_{\text{comp}}E_{\text{comp}}a_{\text{comp}}\Delta\text{T}_{\text{out}}(1-\nu_{\text{liner}})}{2[A_{\text{liner}}E_{\text{liner}}(\nu_{\text{comp}}-1) + A_{\text{comp}}E_{\text{comp}}(1-\nu_{\text{liner}})]} \tag{18}$$

where E_{comp}, a_{comp} and ν_{comp} are the in-plane equivalent moduli, CTE and Poisson's ratio of the laminate (derived from Classical Laminate Theory) and $\Delta\text{T}_{\text{inner}}$ and $\Delta\text{T}_{\text{out}}$ are temperature differences at the boundaries of the inner body (liner) and outer body (composite). This equation could incorporate the respective insulation parameters, where then the insulation properties and ΔTi entities will be multiplied with different terms.

For the case of the composite shell, the total stresses are calculated by:

$$\begin{bmatrix}\sigma_{\text{x}}\\ \sigma_{\text{y}}\\ \tau_{\text{xy}}\end{bmatrix} = \mathbf{C}(\theta)\left(\begin{bmatrix}\varepsilon_x\\ \varepsilon_y\\ \gamma_{xy}\end{bmatrix} - \Delta T\begin{bmatrix}a_{\text{x}}\\ a_{\text{y}}\\ a_{\text{xy}}\end{bmatrix}\right) \tag{19}$$

where α_{x}, α_{y} and α_{xy} are the CTE values of each ply at the same in-plane directions, and by utilizing the transformation matrix $\mathbf{C}(\theta)$ (Eq.4), stress values at each ply at the local materials axis system can be obtained. Equation 18 is utilized in the strain vector of Equation 19.

III. Insulation Configurations

Different design concepts are hereby presented to create a match for the hoop strain between the two bodies. The minimum insulation thickness is calculated, in terms of minimizing the hoop strain of the tank wall. The first concept relies on omitting the insulation (Figure 4a), while the second scenario

is to include it. These cases can be used as reference to the configurations of i) bonded insulation in between the liner and the tank wall and ii) outside of the tank (Figure 4b,c).

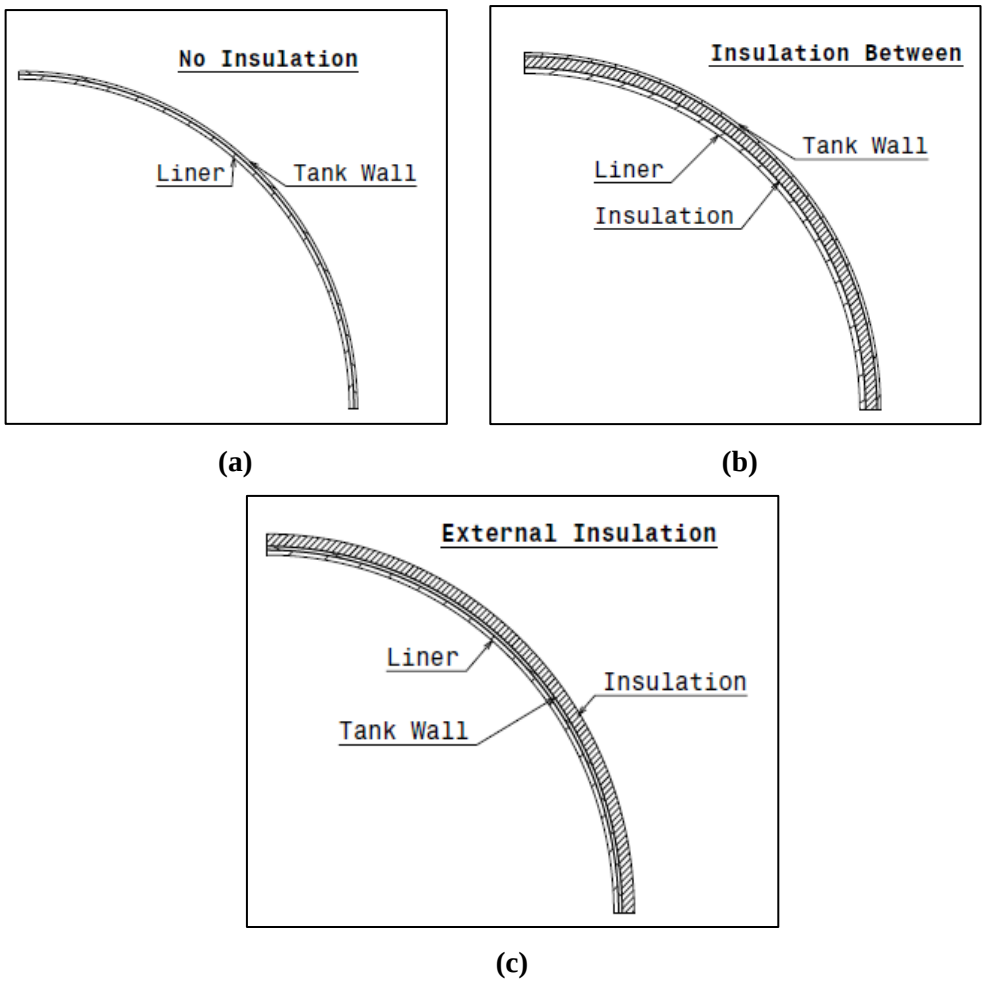

Figure 4: Different tank configurations to alter temperature distributions through-the-thickness: a) no insulation, b) insulation-between and c) external insulation.

The case of internal foam insulation is omitted since this case would provide minimum barrier properties. Table 3 shows the material properties of the employed insulation and liner materials. The liner material PA stands for polyamide.

Table 3: Material properties of employed liner and insulation materials.

Property		Closed-Cell Foam	PA
k	[W K^{-1} m^{-1}]	0.05	0.22
E	[MPa]	10	1008
a	[10^{-6}/°C]	25	90
UTS	[MPa]	15	46

The different tank configurations i) non-insulated, ii) in-between the liner and the tank wall and iii) externally insulated tank) are compared based on the nature of the induced strains and stresses at the liner and the tank wall. A positive strain at the interface leads to the composite shell being loaded axially in tension. Compressive forces should be avoided or minimized at the composite shell, since it

is not desirable to load thin-walled shells in compression. Furthermore the optimal tank configuration will be isolated.

3.2. Intersection Reinforcement

The goal was to identify a reinforcement type that would support the structure at the intersections with the addition of minimum weight. This section deals with analyzing the concept under consideration. A UD carbon tow (roving) can be applied over the tank wall from the outside to the inside under tension, thus forming a ∞ sign (Figure 5). Each hoop fiber-wrapping cycle starts from the top section of the tank between the two ports at the intersection and continues to the central hollow tube covering all unreinforced junctions at longitudinal and circumferential directions. The thickness of the carbon-tow impregnated with resin is considered as 0.3 [mm]. The inner circumference of the central hollow tube should be slightly bigger than the total arc length of all the carbon tows passing through. Additionally the area where the four intersections meet and the circular tube starts, should have high radius of curvature, since the entrapped hoop fibers should be stretched against the tank wall surface. This way the reinforcement will keep the sub-scale tank compact and provide support without adding extra weight to the tank.

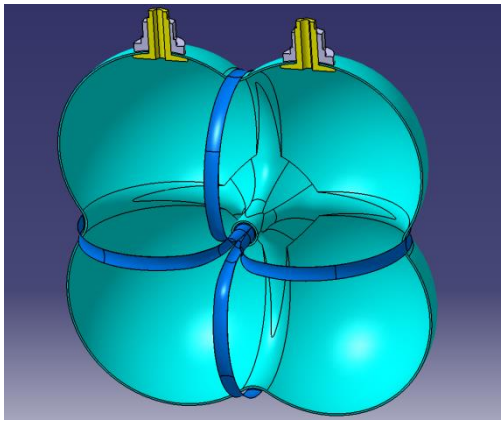

Figure 5: External UD carbon-tow at the intersection.

Analysing the membrane forces can be considered as a three-stage process, when starting from the spherical cell and moving to the intersection, where the highest stress concentrations are expected due to several force components coming into play.

Initially, at the spherical cell (as mentioned above) there is equal biaxial loading and thus the load vector of the laminate at the membrane is given by Equation 20a. However, at the vicinity of the junction, another meridional force component is added at the load vector: the tensile stress resultant at the ring (Figure 6) which is gradually increasing over arc length. At the hoop direction (Figure 6b), where the ring can be considered to be loaded under external pressure, a compressive stress resultant is added, but it is counteracted by the tension coming from both spherical cells. Finally, when approaching the tip of the intersection, the second meridional force generated from the adjacent spherical cell is added, thus having the maximum stress concentration at the tip of each junction. Furthermore it is clear that the structure is loaded in tension at meridional and hoop directions, with the hoop membrane force per unit length of curvature being significantly smaller than the meridional one at these locations, due to lower respective shell radius. The corresponding load vectors (per unit length of circumference) can be derived as follows:

$$\begin{Bmatrix} N_x \\ N_y \\ N_{xy} \end{Bmatrix} = \begin{Bmatrix} \frac{PR_{sph}}{2} \\ \frac{PR_{sph}}{2} \\ 0 \end{Bmatrix}, \qquad \begin{Bmatrix} N_{x2} \\ N_{y2} \\ N_{xy2} \end{Bmatrix} = \begin{Bmatrix} (scf)PR_{ring} + \frac{PR_{sph}}{2} \\ \frac{PR_{sph}}{2} - PR_{fillet} \\ 0 \end{Bmatrix}, \qquad \begin{Bmatrix} N_{x3} \\ N_{y3} \\ N_{xy3} \end{Bmatrix} = \begin{Bmatrix} PR_{ring} + PR_{sph} \\ \frac{PR_{sph}}{2} - PR_{fillet} \\ 0 \end{Bmatrix} \tag{20}$$

where N_x, N_y and N_{xy} are the longitudinal, hoop and shear membrane forces, R_{sph} is the spherical cell radius, *scf* is a stress concentration factor (ranging from 0 to 1) when approaching the intersection and its tip, R_{ring} is the radius of the ring at any cross-section at the junction and R_{fillet} is the fillet radius between two cells.

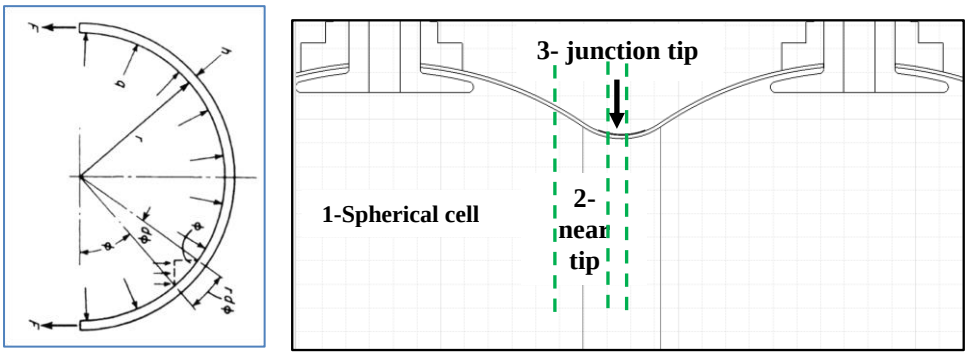

Figure 6: Forces acting at the 2 spherical cells junction [18].

These loads have to be resisted by the laminate and hoop rovings. In order to evaluate the generated stress and strains at each ply, Classical Lamination Theory (CLT) is employed. The stiffness at respective directions defines the stress value, and thus the contribution of each ply to the load support. The axial stress at the hoop fiber is expected to obtain a similar value to that of the 0^o plies, due to almost equal axial stiffness. However the extreme scenario -where the laminate does not provide any local support to the structure and all the load is carried out by the hoop reinforcement- is also taken into consideration. In that case, dividing Equations 20b and c with the hoop fiber thickness returns the axial and transverse average fiber stresses at any point at the membranes.

4 FINITE ELEMENT ANALYSIS OF STRUCTURAL CONFIGURATIONS

4.1. Internal Pressure Only

This section deals with the analysis of different steps that were carried out, as well as the considerations that were taken into account throughout the FE analyses when considering only internal pressure.

A 3D axisymmetric model was built to incorporate the tank wall and study the structural support the reinforcement provides (Figure 7). Solid tetrahedron quadratic 10-node elements (C3D10) were employed at the liner while tri-edron shell elements (S3) were utilized at the composite skin for the simulation with ABAQUS. The unidirectional reinforcement was considered as tied to the composite shell. The maximum expected pressure load (0.57 [MPa]) was applied at the liner inner surface.

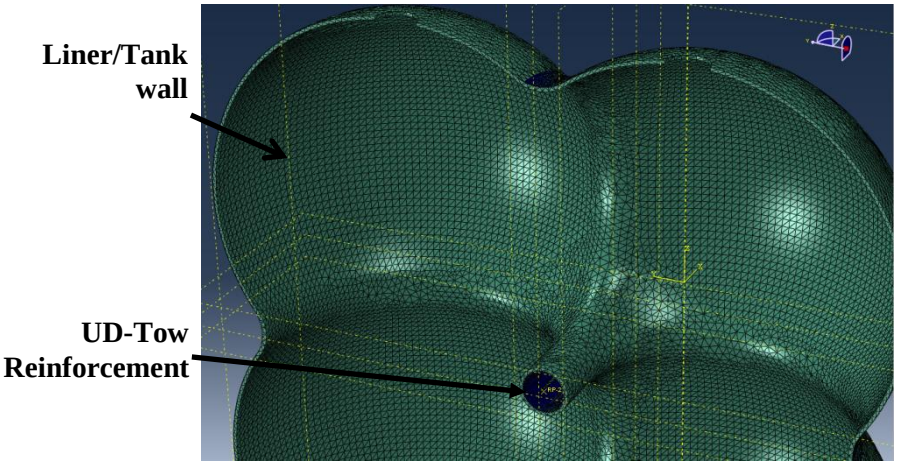

Figure 7: Model part containing the liner and tank wall.

4.2. Thermal/Thermo-mechanical Loading

As mentioned above, it is important to isolate the effect of the thermal loading only- and study the respective tank performance. Therefore, later on, the counter-effect of the internal pressure on the tank can be analysed.

As a result, a coupled temperature-displacement analysis of an eighth of the tank was performed using a FE model, to be representative of the full tank. The tank wall and liner parts had to be partitioned several times through-the-thickness, since a one dimensional steady-state heat transfer process through-the-thickness is expected throughout the analysis. Solid hexagonal linear 8-node elements (C3D8T) were employed at the liner and the tank wall for the simulation run by ABAQUS. The external liner and internal composite surfaces were considered tied throughout the analysis. The tank was subjected to all three loading scenarios as outlined in section 2 (by omitting the pressure load). Temperature loading was introduced at the inner surface in the form of a dedicated boundary condition and the external surface through applying a heat transfer coefficient, depending on the load case. However, for the case of thermo-mechanical loading, the pressure load was applied at the tank inner surface.

Finally, an allowable operating window is established for the proposed tank design by employing all tank configurations of interest, having as variables: i) external temperature and the ii) inner pressure, since inner temperature was considered as -253 [^{o}C]. This analysis is carried out for the case that the laminate contributes in carrying the radial load at the intersection, so that it is not carried solely by the hoop fiber (the ∞-shaped roving).

5 RESULTS

This section contains the results on the subscale tank for i) internal pressure only, ii) thermal and iii) thermo-mechanical loading.

5.1. Pressure Only

As mentioned above, two distinct cases were considered when analyzing the effect of internal pressure on the tank behavior: i) with and ii) without laminate stiffness contribution at the junctions.

Figure 8a depicts the axial and circumferential stress distribution at the spherical membrane and junction of the first ply at the composite tank wall for the highest expected internal pressure with a safety factor of 1.5 (SF = 1.5). The outer ply (0[^{o}]) was chosen for visualization, since the highest stress values were obtained due to its high stiffness in axial direction. A good correlation between analytical and FE solutions can be seen. It is evident that the axial stress at the junction –where there are two different force components (Section 3.2)- increases significantly. Figure 8b illustrates the exerted axial stress at the UD carbon tow where, it is clear that at most regions of the hoop fiber the axial stress is at the vicinity of the peak stress at the 0[^{o}] plies of the laminate, with the intersection of

the four fibers sustaining the highest stress at 270 [MPa]. Under this scenario the maximum allowable pressure is 3.1 [MPa] (31 [bar]), with FPF occurring at the 90[^{o}] plies.

On the other hand, in the case that there is no laminate contribution at the intersections, this leads to the UD reinforcement carrying the full load at the junctions, leading to a lower tank maximum allowable pressure that is directly linked to the hoop reinforcement thickness, but this scenario is an extreme. Figure 8c shows that the axial stress (in [MPa]) has increased twice in value, since the hoop fiber is resisting the full radial load and thus has higher tensile stresses.

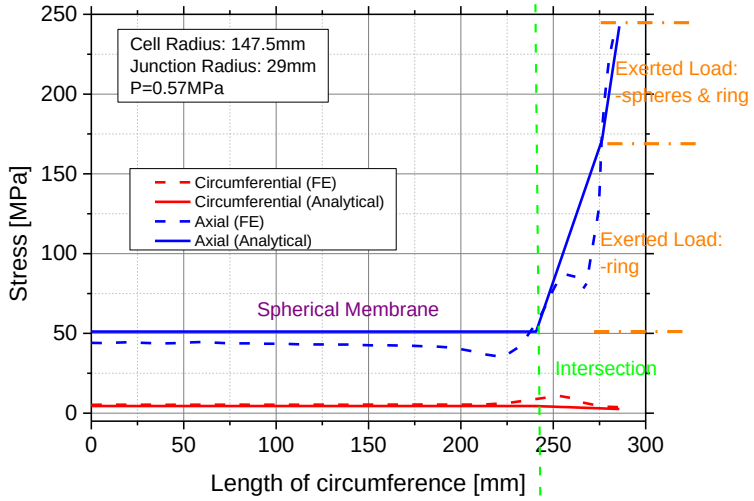

(a)

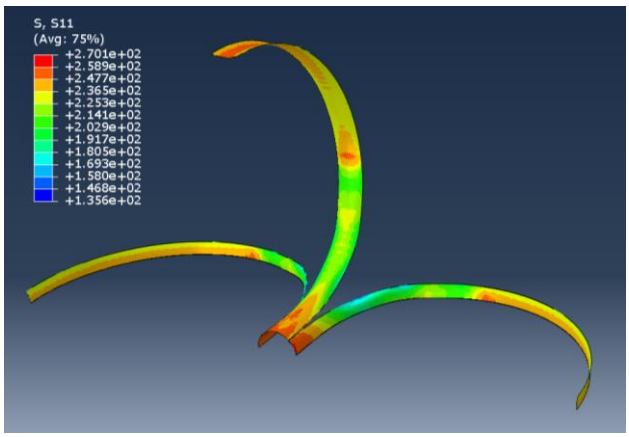

(b)

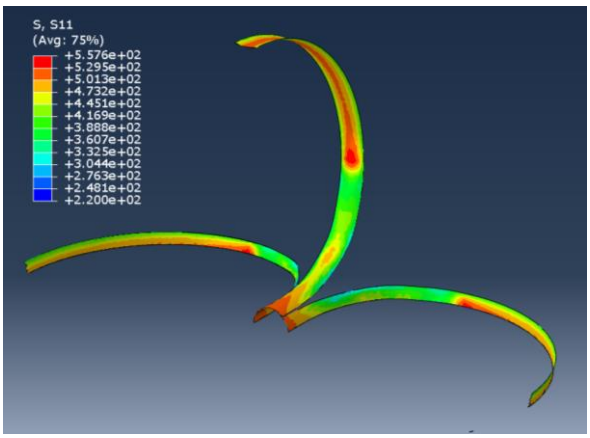

(c)

Figure 8: a) Axial and circumferential stresses at the spherical cell and intersection for ply 0 and b) axial stress for the UD fiber for *P* = 0.57 [MPa]. c) Extreme case: UD reinforcement axial stress without any laminate stiffness contribution at the junctions for *P* = 0.57 [MPa].

5.2. Thermal Loading

Figure 9 shows a good correlation between the analytical solution and the FE solution for the temperature distribution of the liner and composite shell through-the-thickness at all three tank load cases when isolating the thermal loading. Furthermore, the axial and transverse stress distributions due to thermal loading are depicted. The initial temperature used was room temperature. As expected, the tank wall in all load cases is subjected to compressive stresses in the axial direction and tensile stresses in the transverse direction, due to the fact that the interfacial strain (Eq.18) is negative. In case the liner and tank wall would not be initially tied, that would lead to liner/tank wall separation which should be avoided, since the liner only then would have to carry the pressure load.

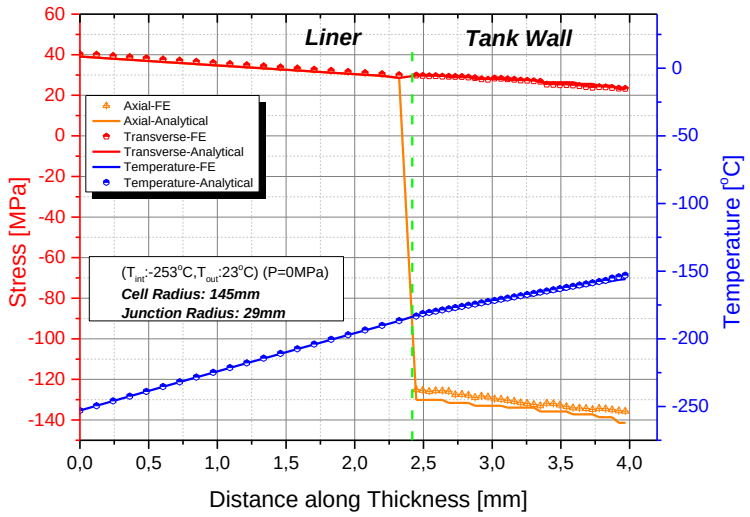
Liner
Tank Wall
Axial-FE
Axial-Analytical
Transverse-FE
Transverse-Analytical
Temperature-FE
Temperature-Analytical
(T_int:-253°C,T_out:23°C) (P=0MPa)
Cell Radius: 145mm
Junction Radius: 29mm
Stress [MPa]
Temperature [°C]
Distance along Thickness [mm]

(a)

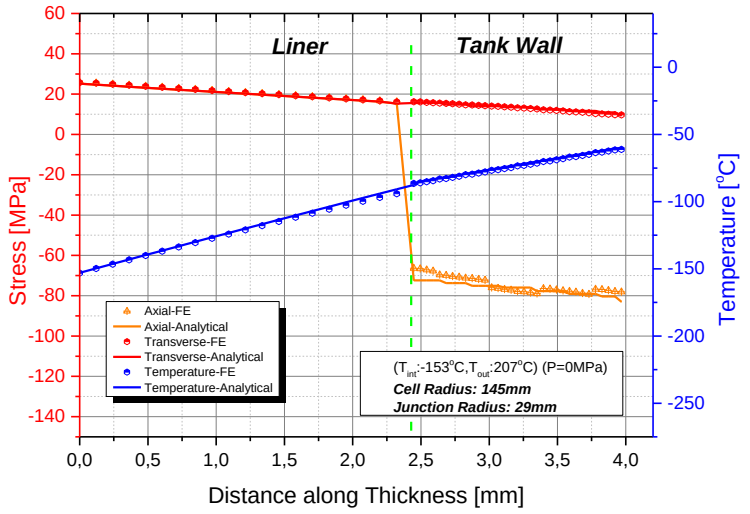
Liner
Tank Wall
Axial-FE
Axial-Analytical
Transverse-FE
Transverse-Analytical
Temperature-FE
Temperature-Analytical
(T_int:-153°C,T_out:207°C) (P=0MPa)
Cell Radius: 145mm
Junction Radius: 29mm
Stress [MPa]
Temperature [°C]
Distance along Thickness [mm]

(b)

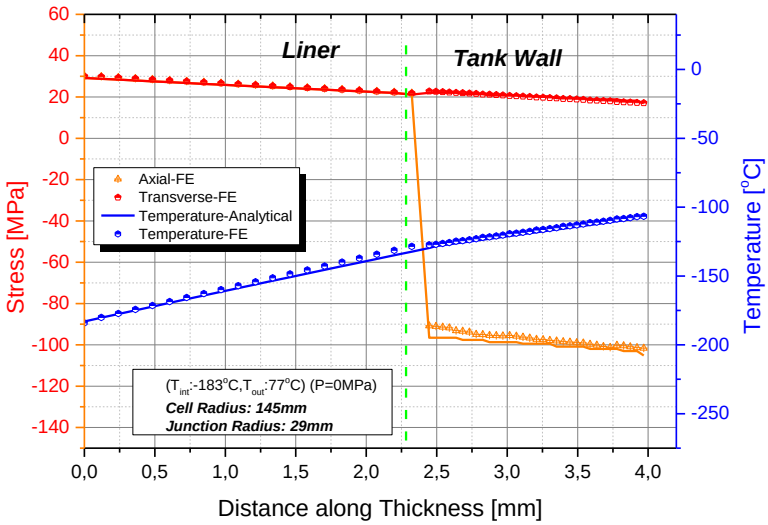
Liner
Tank Wall
Axial-FE
Transverse-FE
Temperature-Analytical
Temperature-FE
(T_int:-183°C,T_out:77°C) (P=0MPa)
Cell Radius: 145mm
Junction Radius: 29mm
Stress [MPa]
Temperature [°C]
Distance along Thickness [mm]

(c)

Figure 9: Temperature and axial thermal stress distribution through-the-thickness for the liner and composite shell for the a) normal cryogenic operation, b) nominal empty operation after MECO at maximum expected outside temperature and c) off-nominal operation after early MECO with remaining LH_2.

5.3. Thermo-mechanical Loading

For the case of combined loading, the inner pressure above a certain value causes a positive net radial expansion to the liner, thus forcing it to come in contact with the tank wall. This induces full load and heat transfer to the laminate. Therefore it is analysed where contact can be achieved within a given load regime, without bonding the two surfaces together and without adding any insulation.

Initially it has to be evaluated which pressure and liner upper surface temperature is needed to achieve the desired liner hoop strain values under normal LH_2 storage conditions. The net hoop strain value needs to be larger than 0 [%]. Figure 10a depicts the required interfacial temperature and inner pressure in order to reach liner/tank wall contact, for varying liner external temperature and inner pressure values. In order to achieve a hoop strain of 0 [%], the pressure needs to be 1.21 [MPa] approximately for cryogenic temperatures while almost 0.77 [MPa] for interfacial temperatures near -50 [^{o}C], revealing the linear trend of the strain behavior and the fact that there must a higher temperature at the liner external surface. However, this is outside of the load regime shown in Figure 1 and before even achieving contact the pressure is going to carried by the liner which will eventually crack, due to carrying the full pressure and thermal load. Therefore effective insulation systems need to be employed at the design- in order to alternate this behavior.

Figure 10b illustrates the required liner tensile modulus and CTE, in order to achieve contact with the tank wall, when the first load case is analysed by employing equation 18. The symbol T_{in} signifies the temperature at the inside of the liner and T_{out} the temperature at the outside of the composite. A non-linear trend can be observed; it is clear that most plastics do not fall within this framework.

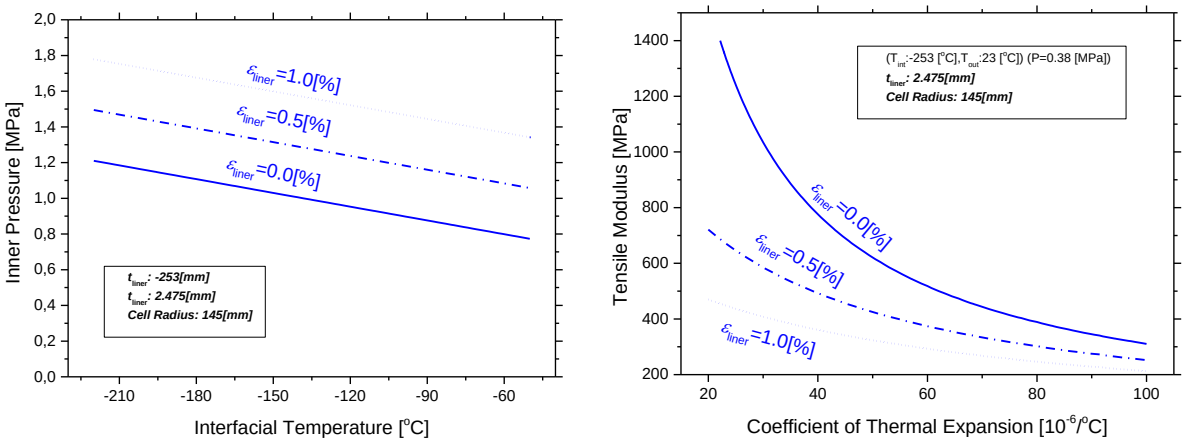

(a) **(b)**

Figure 10: Contour plots of a) required interfacial temperature and inner pressure and b) required liner material properties for a prescribed inner pressure, to achieve liner/tank wall contact.

As mentioned in Section 3.1.2, in order to tackle this issue, various thermal insulation systems were taken into consideration and compared with the non-insulated case. The main focus was to minimize the absolute value of strain at the liner/tank wall or insulation/tank wall interface thus decreasing compressive axial and tensile transverse stresses at the tank wall, which leads to minimisation of the failure criterion for each ply. Figure 11a illustrates a comparison between the interfacial hoop strain for all systems in this study: (i) in-between insulation, ii) external insulation and iii) without any insulation for the normal cryogenic operation case. It is evident that external insulation leads to a increase of the absolute value of hoop strain in a non-linear manner, while in-between insulation has

the opposite effect. This can be explained by the fact that the external insulation introduces a thermal barrier between the atmosphere and the tank, thus lowering the temperatures through-the-thickness, which results to higher shell contraction.

Figure 11b shows the correlation between the insulation thickness and the dimensionless ratio of generated Von Mises stress in conjunction with the liner material tensile strength, thus describing the rate of liner failure. This ratio is mainly liner material property-driven, and it is generally required to employ a plastic with low tensile modulus and high strength value. It can be seen that none of the tank configurations -under study- leads to liner failure, despite the fact that a low safety factor was obtained for all cases. In-between insulation has a negative effect on the liner structural integrity, which can be associated to the fact that the liner is isolated from the composite and is only in contact with the cryogenic propellant and the insulation.

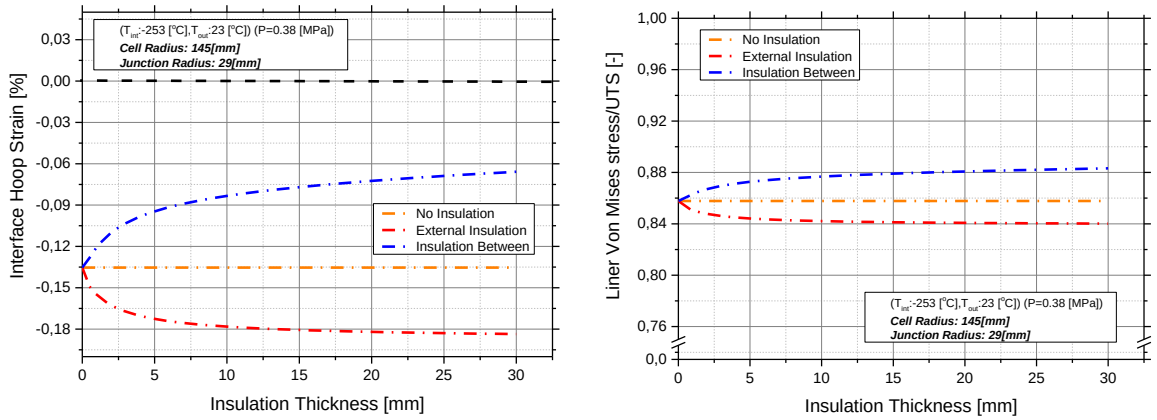

Figure 11: Comparison of different tank configurations for the normal cryogenic operation based on the a) hoop strain at the liner/tank wall interface and b) the liner performance.

Figure 12a illustrates a comparison between the axial and transverse stresses at the inner ply (0[^{o}]) for all the configurations of interest. The inner ply was chosen since it consists of the highest failure criterion value. It can be seen that the non-insulated case leads to an axial compressive stress of -102 [MPa], while the externally-insulated case further decreases the compressive axial and increases the tensile transverse stresses values with the addition of more insulation. The effect of tension due to internal pressure can be shown in the values of axial and transverse stresses in Figure 12a compared to Figure 9a for the non-insulated case. On the contrary, lower axial compressive and tensile transverse stresses can be maintained with an in-between insulation while the failure criterion value becomes minimized as compared to the other two configurations. A global minimum is achieved for 15 [mm] insulation thickness for this tank configuration.

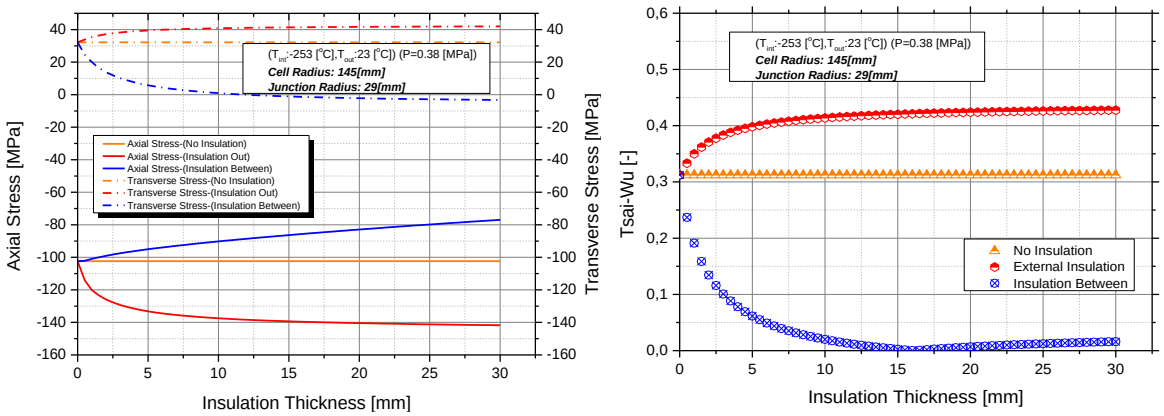

Figure 12: Comparison of different tank configurations for the normal cryogenic operation based on the generated axial and transverse stresses and respective failure criterion of the inner composite ply.

Figure 13 illustrates an operating window for the cryogenic tank based on either i) liner failure or ii) first-ply failure, where the location of failure is at the intersections. All tank configurations were taken into consideration and the temperature of LH_2 boiling point (-253 [^{o}C]) was applied at the tank inner wall. Insulation was chosen to be as thick as 15 [mm], since it was shown at Figure 12b that it leads to a failure criterion minimum. It can be seen that an outer temperature range of 23 [^{o}C] < T_{out} < 207 [^{o}C] was chosen, since this temperature range is a representative for the extremes that the tank can be subjected to, given the flight stage loading scenarios (Figure 1). As expected, the 90[^{o}] plies are failing first in two tank configurations (namely for the non-insulated and externally insulated), thus defining the lowest pressure allowable over varying outer temperatures. It is evident that for these two cases when increasing T_{out} then the pressure allowable increases. The in-between insulation shows the best performance, with a maximum pressure allowable reaching 1.71 [MPa], approximately for T_{out} = 23 [^{o}C], while external insulation shows the worst performance, where the minimum inner pressure allowable (1.02 [MPa] at 23 [^{o}C]) was obtained. Unlike the previous two cases, the failure pattern of the in-between insulation relies on liner failure and the pressure allowables have a decreasing trend with increasing outer temperature. Finally it is clear that the pressure allowable values of all tank configurations are well above the one given by the tank operation requirements of Figure 1.

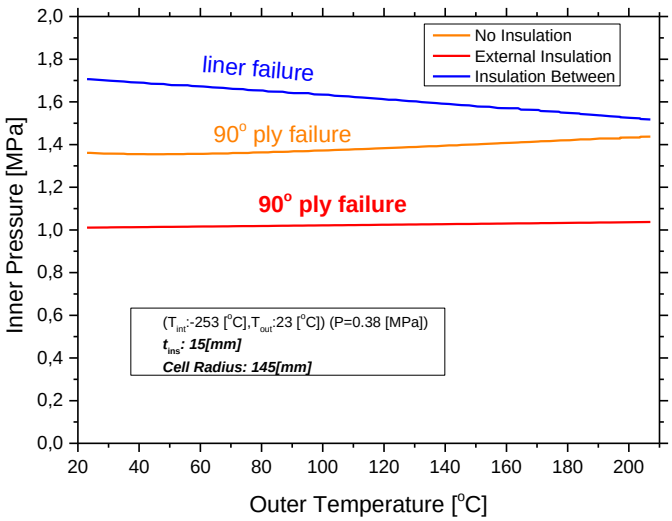

Figure 13: Operating window for the tank under thermo-mechanical loading (normal cryogenic operation).

6 CONCLUSIONS

In the current study, the effect of the i) fiber-reinforced materials at the membrane and ii) unidimensional carbon tows at the intersections on the structural integrity of the tank was analysed for different thermo-mechanical loading scenarios. The goal was to provide effective reinforcement at the intersections and polar openings for filling and draining of the tank, and evaluating, by using FE analysis, the structural behavior of the tank under internal pressure and thermal loading. Additionally, the concept of minimizing axial and transverse stresses at the composite and liner shell was analysed-through the use of proper liner materials and addition of effective insulation, in order to alternate to temperature and thus strain distribution at both bodies.

The FE and analytical solution results have shown that there is a very uniform biaxial loading of the spherical cells and localized stress concentrations junction of the membranes. Furthermore, the temperature distribution and respective thermo-mechanical stresses at the liner and composite shell were evaluated, based on heat conduction between the liner and tank wall and convection with air. Different insulations systems were analysed to quantify their effect on the arising stresses and strains. A safe operating window for the tank for different tank configurations was established for the case of normal cryogenic operation. It was shown that the tank pressure allowable decreased significantly when storing cryogenic propellant (liquid hydrogen), compared to storing mediums at room temperature but is still well above the one given by the tank operation requirements. Finally it was shown that the tank structural integrity is enhanced by utilizing insulation between the liner and the composite.

ACKNOWLEDGMENTS

This work has been performed within the 'Cryogenic Hypersonic Advanced Tank Technologies' project investigating tank technologies for high-speed transport. CHATT, coordinated by DLR-SART, is supported by the EU within the 7th Framework Program Theme 7 Transport, Contract no.: ACP1-GA-2011-285117. Further information on CHATT can be found on http://www.chatt.aero.

REFERENCES

[1] M. Sippel and A.van Foreest, 'SpaceLiner Rocket-Powered High-Speed Passenger Transportation Concept Evolving in FAST20XX', *Proceedings of the 61st International Astronautical Congress*, Prague, 2010.

[2] F.J.J.M.M. Geuskens, O.K. Bergsma, S. Koussios and A. Beukers, Analysis of Conformable Pressure Vessels: Introducing the Multibubble, *AIAA Journal*, **49**, 2011, pp. 1683-1691.

[3] A. Haaland, High-Pressure Conformable Hydrogen Storage for Fuel Cell Vehicles, *Proceedings of the U.S. DOE Hydrogen Program Review, California*, 2000, 463-469.

[4] V.V. Vasiliev, *Composite Pressure Vessels: Analysis, Design and Manufacturing*, Bull Ridge Publishing, 2009.

[5] C.C. Liang, S.W. Shiah, C.Y. Jen and H.W. Chen, 'Optimum design of multiple intersecting spheres deep-submerged pressure hull', *Ocean Engineering*, **31**, 177–199, 2004.

[6] G.F. Leon, 'Advanced Hull Design - Intersecting Titanium Spheres', *Proceedings of the Offshore Technology Conference*, Texas, 1969.

[7] 'Final Report of the X-33 Liquid Hydrogen Tank Test Investigation', NASA Marshall Space Flight Center, Huntsville, 2000.

[8] T.F. Johnson, W.A. Waters, T.N. Singer and R.T. Haftka, 'Thermal–structural optimization of integrated cryogenic propellant tank concepts for a reusable launch vehicle', *AIAA Journal*, **6**, 4416-4426, 2004.

[9] S.M. Aceves, G.D. Berry and G.D. Rambach, 'Insulated pressure vessels for hydrogen storage on vehicles', *International Journal of Hydrogen Energy*, **23**, 583-591, 1998.

[10] T.C. Nast, D.J. Frank and J. Feller, 'Multilayer insulation considerations for large propellant tanks', *Cryogenics*, **64**, 105–111, 2014.

[11] A.K. Majumdar, T.E. Steadman and J.L. Maroney, 'Numerical Modeling of Propellant Boiloff in Cryogenic Storage Tank', *NASA Technical Report*, 2007.

[12] M. Sippel, A. Kopp, K. Sinko and D. Mattsson, 'Advanced Hypersonic Cryo-Tanks Research in CHATT', *Proceedings of the 18th AIAA International Space Planes and Hypersonic Systems and Technologies Conference*, France, 2012.
[13] W. Flügge, *Stresses in Shells*, Springer- Verlag Berlin Heidelberg GmbH, 1960.
[14] S.T. Peters, *Composite Filament Winding*, ASM International Materials Park, 2011.
[15] G.D. Raithby, K.G.T. Hollands, 'A general method of obtaining approximate solutions to laminar and turbulent free convection problems', *Advances in Heat Transfer*, **11**, 265–315, 1975.
[16] N. Noda, R.B. Hetnarski and Y. Tanigawa, *Thermal Stresses*, Taylor & Francis, 2003.
[17] A.C. Ugural, *Stresses in Plates and Shells*, McGraw-Hill, 1981.
[18] D.M. Fryer and J.F. Harvey, *High Pressure Vessels*, Chapman & Hall, 1998.